Analyst

RSC Publishing

PAPER

View Article Online
View Journal | View Issue

Cite this: *Analyst*, 2013, **138**, 5417

Carbon dots and chitosan composite film based biosensor for the sensitive and selective determination of dopamine

Qitong Huang,[a] Shirong Hu,*[ab] Hanqiang Zhang,[a] Jianhua Chen,[ab] Yasan He,[a] Feiming Li,[a] Wen Weng,[ab] Jiancong Ni,[a] Xiuxiu Bao[a] and Yi Lin[a]

Received 14th March 2013
Accepted 23rd May 2013

DOI: 10.1039/c3an00510k

www.rsc.org/analyst

A simple, sensitive and reliable dopamine (DA) biosensor was developed based on a carbon dots (CDs) and chitosan (CS) composite film modified glassy carbon electrode (CDs–CS/GCE). Under optimal conditions, the CDs–CS/GCE showed a better electrochemical response for the detection of DA than that of the glassy carbon electrode (GCE). The oxidation peak current (I_{pa}) of DA was linear with the concentration of DA in the range from 0.1 μM to 30.0 μM with the limit of detection as 11.2 nM (3*S*/*N*). The CDs–CS/GCE was applied to the detection of DA content in an injection solution of DA with satisfactory results.

1 Introduction

Acting as a neuromodulator of ionotropic synapses, dopamine (DA) sets a threshold for striatal activity, it is also involved in some diseases and in drug addiction. In addition, DA is available as an intravenous medication, which acts on the sympathetic nervous system, to produce effects such as increasing heart rates and blood pressure.[1–5] Hence, determination of DA *in vivo*/*vitro* becomes increasingly important in clinical medical practice. In recent years, several instrumental methods for DA determination have been developed, such as high performance liquid chromatography,[6,7] ultraviolet-visible spectrophotometry,[8] capillary electrophoresis,[9–11] fluorescence spectrometry[12,13] and electrochemical methods[14–26] *etc.* Moreover, compared with other described methods, the direct electrochemical method for DA analysis, as a simple, rapid, and sensitive alternative, is drawing increasing attention. Thus, more and more materials have been used to modify the electrodes to detect DA, such as graphene (GME),[14] methoxypolyethylene glycol (MPEG),[15] hollow nitrogen-doped carbon microspheres (HNCMS/GC),[16] a Cu_2O/graphene nanocomposite (Cu_2O/graphene),[17] Au nanoparticle–polyaniline nanocomposite layers (AuNP/PANI),[18] tetrabromo-*p*-benzoquinone (TBQ/MCPE),[19] a nanoporous morphology of a gold nanofilm (NPG/ITO),[20] multiwalled carbon nanotubes (f-MWCNTs),[21] polypyrrole and graphene (PPy/eRGO),[22] a 3-amino-5-mercapto-1,2,4-triazole self-assembled monolayer (TA-SAM),[23] *O*-carboxymethylchitosan (OCMCS),[2,4] and carbon fibre microelectrodes.[25,26] Although most of these systems made many contributions for the detection of DA, these modified materials had either limitations with respect to sensitivity or the material synthesis was sophisticated and expensive. Consequently, it is highly desirable to develop a sensor that is not only sensitive, selective and reliable but also simple, practical, and economical in biological, pharmacological and toxicological applications.

Carbon dots (CDs) are a class of 'zero-dimensional' carbon nanomaterials that have recently received considerable attention because of their advantageous characteristics, such as excellent water solubility, biocompatibility and good photostability, these features make CDs especially useful for fluorescent biosensing or imaging.[27,28] However, the exploration of CDs as electrochemical sensors to monitor analytes with high selectivity and sensitivity still remains at an early stage.[29] Compared with other electrode modified materials, the electrochemical research of CDs will gain more and more importance due to the low cytotoxicity, excellent biocompatibility, simple synthesis, economy and remarkable conductivity. Herein, we report a new quantitative method for rapid, simple and sensitive determination of DA. It is aimed at the development of a CS and CDs composite film modified GCE for the determination of trace amounts of DA with high sensitivity. The CDs synthesized by microwaves have carboxyl and hydroxyl groups.[28] Therefore, this demonstrates that the hybrid film could significantly enhance the redox response of DA, and under optimal conditions good linearity was observed between the differential pulse voltammetric peak current and the concentration of DA in the range from 0.1 μM to 30 μM in pH 7.0 phosphate buffer solution.

[a]*Department of Chemistry and Environment Science, Zhangzhou Normal University, Zhangzhou 363000, PR China. E-mail: Hushirong6666@163.com; Fax: +86 596 2528075; Tel: +86 596 2528075*

[b]*Fujian Province University Key Laboratory of Analytical Science, Zhangzhou Normal University, Zhangzhou 363000, PR China*

2 Experimental

2.1 Reagents and instrumentation

Glucose, glacial acetic acid, ascorbic acid and polyethylene glycol-200 were purchased from Xilong Chemical Co., Ltd. (Guangdong, China), phosphate buffer solution was from Shanghai Kangyi Instrument Co., Ltd. (Shanghai, China), chitosan, uric acid, serotonin, norepinephrine and dopamine were obtained from Sinopharm Chemical Reagent Co., Ltd. (Shanghai, China). All other reagents are analytical reagents. Nanopure deionized and distilled water (18.2 MΩ) was used throughout all experiments.

Electrochemical experiments such as cyclic voltammetry (CV), electrochemical impedance spectroscopy (EIS) and differential pulse voltammetry (DPV) were carried out on a CHI 650D electrochemical workstation (Shanghai ChenHua Instruments Co., China). A conventional three-electrode system was used for all electrochemical experiments, which consisted of a platinum wire as the auxiliary electrode, an Ag/AgCl/saturated KCl as the reference electrode, and a bare or modified GCE as the working electrode. The pH measurements were carried out on a pHS-3C exact digital pH metre (Shanghai Mettler-Toledo Instruments Co., Ltd), which was calibrated with standard pH buffer solutions. The fluorescence spectra were recorded by a Varian Cary Eclipse fluorescence spectrophotometer with a 1.0 cm quartz cell (Ex slit 10 nm, Em slit 10 nm). The UV-vis absorption was registered by mapada UV-1800PC (Shanghai China). The surface morphology of the CDs–CS film was observed with atomic force microscopy (AFM, CSPM5500, China). Transmission electron microscopy (TEM) was performed on a JEM-1230 electron microscope (JEOL, Ltd., Japan) at 300 kV. A microwave oven (Galanz) and an AE240 electronic analytical balance (Shanghai Mettler-Toledo Instruments Co., Ltd) were used. All experiments were conducted at room temperature.

2.2 Synthesis of CDs

10.00 mL of polyethylene glycol-200 (PEG-200) and 2.0000 g of glucose were mixed and dissolved in 3.00 mL of water to form a pellucid solution. Then the mixture was put into a 540 W microwave oven, two minutes later, a yellow CDs solution was obtained.[27] Lastly, the CDs were dialyzed for 24 h with the dialysis membranes of 1000 cutoffs and diluted to 50.00 mL with water, then stored at 4 °C ready for use.

2.3 Electrode preparation

The GCE was polished to a mirror-like surface with a 1.0 μm, 0.3 μm, and 0.05 μm α-alumina slurry, and then washed successively with distilled water, ethanol and distilled water in an ultrasonic bath, and dried in air before use.

Synthesis of the CDs–CS composite film: 1 mL of 1.0% CS solution was added to 3 mL of CDs solution with vigorous ultrasonication. Then with a micro injector, 9.0 μL of the mixture solution was cast on the surface of the GCE, and left to dry in an oven at 60 °C for 30 min.

3 Results and discussion

3.1 Characterization of CDs and CDs–CS/GCE

The morphology of the CDs was characterized by TEM (Fig. 1A), typical UV-vis absorption spectra and fluorescence spectra of the CDs are shown in Fig. 1B. A strong absorption band appears at 282 nm; the fluorescence excitation and emission wavelengths appear at 344 and 432 nm. These values were consistent with previous reports.[27,30]

AFM images of the bare GCE and the CDs–CS/GCE film are shown in Fig. 2. They show that the bare GCE surface is relatively smooth with an average roughness of 1.13 nm (Fig. 2A) whereas the average roughness of the GCE is 17.3 nm after modification by CDs–CS (Fig. 2B), where irregular round islands appeared, which explains how the surface morphology changed the roughness. This result demonstrated that the CDs–CS film was deposited on the GCE surface.

3.2 Electrochemical properties of the CDs–CS/GCE electrode

The $[Fe(CN)_6]^{3-/4-}$ redox couple was used for electrode characterization and the electrochemical response from the Fe^{3+}/Fe^{2+} redox couple could reflect the conductivity of the electrode interface. The electrochemical behaviors of different modified electrodes were investigated in a 1.0 mM $K_3[Fe(CN)_6]$ and 0.1 M KCl mixed solution with cyclic voltammetry (CV), as shown in Fig. 3A. At the bare GCE (a), a pair of redox peaks appeared. After casting CS onto the GCE (b), the redox peaks increased a little, which could be attributed to the affinity of positively charged CS to negatively charged $[Fe(CN)_6]^{3-/4-}$. When the CDs–CS was fixed onto the GCE surface (c), the redox peaks increased obviously, which was due to the excellent electrical conductivity of the CDs–CS present on the electrode's surface. In summary, the CDs–CS composite film has a large surface area and a high conductivity, which can accelerate the electron transfer rate.

By investigating the CV of the CDs–CS/GCE in $K_3[Fe(CN)_6]$ solution with varied scan rates, the slope of the linear regression between the current and the square root of the scan rate can be described by Randles–Sevcik's equation.[31]

$$I_{pa} = 2.69 \times 10^5 n^{3/2} A C_0 D v^{1/2}$$

where I_{pa} refers to the anodic peak current, n is the electron transfer number, A is the surface area of the electrode, D is the

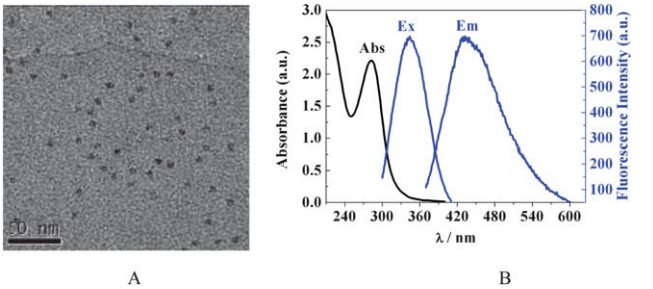

Fig. 1 (A) TEM image of the CDs (B) UV-vis absorption spectra (Abs) and fluorescence spectra (Ex, Em) of the CDs intensity.

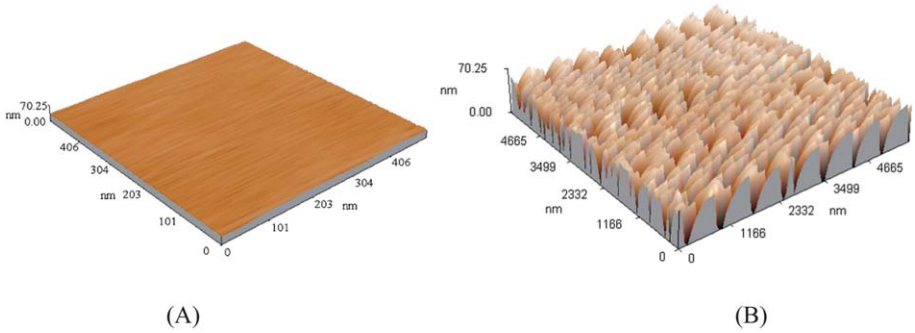

Fig. 2 (A) AFM image of the bare GCE (B) AFM image of the CDs–CS/GCE.

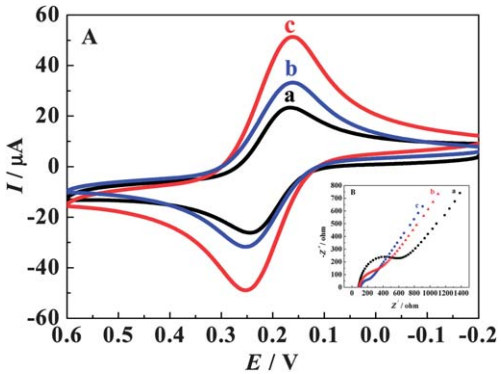

Fig. 3 CV (A) and EIS (B) of 1.0 mM $[Fe(CN)_6]^{3-/4-}$ recorded on the bare GCE (a), the CS/GCE (b) and the CDs–CS/GCE (c).

diffusion coefficient, C_0 is the concentration of $K_3Fe(CN)_6$ and ν is the scan rate. For 1.0 mM $K_3Fe(CN)_6$ in the 0.1 M KCl electrolyte: $n = 1$ and $D = 7.6$ μcm s^{-1} then from the slope of the I_{pa}–$\nu^{1/2}$ relationship, the microscopic areas were calculated. For the bare GCE, the electrode surface was found to be 0.039 cm^2 and for the CDs–CS/GCE the surface was 0.094 cm^2, which increased nearly 2.3 times.

Electrochemical impedance spectroscopy (EIS) was further used for the investigation of the modified electrodes, it can exhibit the impedance changes of the modification processes. The value of the electrode-transfer resistance (R_{et}) depends on the dielectric and insulating features at the electrode–electrolyte interface. Fig. 3B shows the EIS of different electrodes in 1.0 mM $[Fe(CN)_6]^{3-/4-}$ and 0.1 M KCl solution. On the GCE (a) the R_{et} value was 600 Ω. While on the CS/GCE (b) the R_{et} value was decreased to 350 Ω, indicating that the presence of CS on the electrode surface could accumulate more $[Fe(CN)_6]^{3-/4-}$ and accelerate the diffusion of ferricyanide towards the electrode surface. However, on the CDs–CS/GCE (c), the R_{et} value was greatly decreased to 130 Ω, which could be attributed to the presence of high conductivity CDs in the composite film that accelerated the electron transfer rate of $[Fe(CN)_6]^{3-/4-}$. Hence, the appearance of CDs in the modified film could depress the resistance of the sensing platform in the solid and solution system, thus an accelerated rate of electron transfer of $Fe(CN)_6^{3-/4-}$ was obtained. This also strongly proves that the CDs–CS composite film could be a promising electrochemical platform for sensing.

3.3 Cyclic voltammetric behavior of DA on the CDs–CS/GCE

The electrochemical response of DA at the GCE, the CS/GCE and the CDs–CS/GCE was examined using CV in a 0.2 mM DA solution. As shown in Fig. 4, when the CDs–CS was fixed on the GCE surface, the redox peaks increased obviously, benefiting from the unique properties of the CDs and CS, the CS backbone together with the CDs introduced an obviously sensitized effect toward the electrochemical redox of DA. Hence, this electrochemical platform based on CS and CDs offers the enhanced determination sensitivity for DA. A possible reaction mechanism of the CDs–CS/GCE with DA is discussed, which is shown in Scheme 1. CS is a biological cationic macromolecule with primary amines, and there are diols, amine functional groups, and phenyl in the DA molecules, therefore, the direct reaction between DA and CS might not ocurr.[32] However, the CDs synthesized by microwaves have carboxyl groups with a negative charge, which not only provides good stability but also enables interaction with the amine functional groups in DA through electrostatic interaction to recognize DA with high specificity.

3.4 The diffusion coefficient of DA on the CDs–CS/GCE

Chronocoulometry was employed to determine the diffusion coefficient of DA on the CDs–CS/GCE. After subtracting the

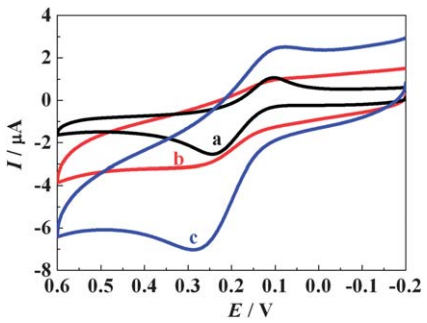

Fig. 4 CV of 0.2 mM DA recorded on the bare GCE (a), the CS/GCE (b) and the CDs–CS/GCE (c) in a pH 7.0 phosphate buffer solution (scan rate: 0.1 V s^{-1}).

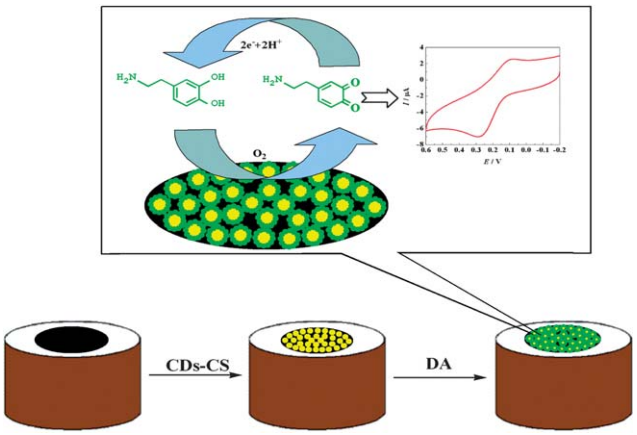

Scheme 1 Schematic illustration of the strategy for DA detection.

background in the pH 7.0 phosphate buffer solution, the charge (Q) on the CDs–CS/GCE against the time (t) can be described by the following equation given by Anson:[33]

$$Q = \frac{2nFAcD^{1/2}t^{1/2}}{\pi^{1/2}} + Q_{ads}$$

where A is the surface area of the working electrode, n is the electron transfer number, D is the diffusion coefficient, Q_{ads} is faradic charge, other symbols have their normal meaning. As is described in Fig. 5, based on the slope of the linear relationship between Q and $t^{1/2}$, the diffusion coefficient of DA can be calculated to be 3.68×10^{-6} cm^2 s^{-1}, which illustrates a relatively fast electrode reaction process of DA on the electrochemical platform based on CDs–CS.

3.5 Effects of scan rate

The effect of the scan rate on the redox of DA was also investigated. Fig. 6A reveals the CV of 0.2 mM DA at the CDs–CS/GCE with different scan rates. The redox peak current increased gradually with the increase in scan rate. As shown in Fig. 6A, the redox peak current of DA increased linearly with the square root of the scan rate in the range of 0.1–1.0 V s^{-1}, which indicated that the electro-redox of DA on the CDs–CS/GCE was a typical diffusion controlled process. Moreover, with the increased scan rate, the redox potential of DA shifted positively. The relationship between the potential and the scan rate can be described by the following equations by Laviron:[34]

$$E_{pa} = E^{0'} + \frac{2.3RT}{(1-\alpha)nF}\log v$$

$$E_{pc} = E^{0'} + \frac{2.3RT}{\alpha nF}\log v$$

$$\log k_s = \alpha\log(1-\alpha) + (1-\alpha)\log\alpha - \log\frac{RT}{nFv} - \frac{(1-\alpha)\alpha nF\Delta E_p}{2.3RT}$$

where α is the electron transfer coefficient, n is the number of transfer electrons, k_s is the standard heterogeneous rate constant, R, T and F have their usual significance, E_{pa} is the oxidation peak potential and E_{pc} is the reduction peak potential. Generally, for an electrochemical reaction, the values of α and n can easily be calculated from the slope of E_{pa} *vs.* log v and E_{pc} *vs.* log v. The linear regression equations were E_{pa} (V) = 0.0911 log v (V s^{-1}) + 0.372 (R = 0.994) and E_{pc} (V) = −0.0578 log v (V s^{-1}) + 0.0206 (R = 0.995), which are shown in Fig. 6B. After making computations: α = 0.61, n = 1.8, k_s = 0.14 s^{-1}.

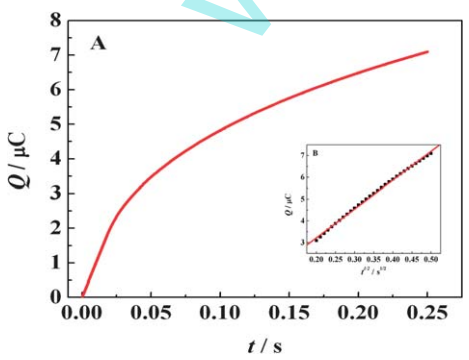

Fig. 5 (A) Chronocoulometry of 0.2 mM DA on the CDs–CS/GCE in a pH 7.0 phosphate buffer solution. (B) Linear relationship between Q and $t^{1/2}$.

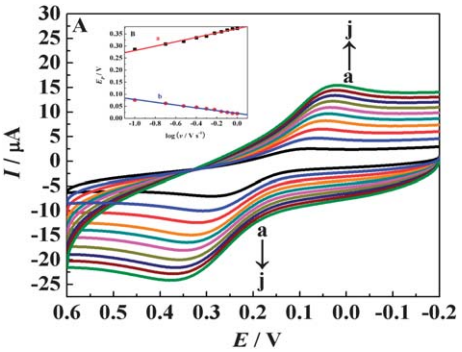

Fig. 6 (A) CV of 0.2 mM DA on the CDs–CS/GCE in a pH 7.0 phosphate buffer solution at various scan rates (a–j: 0.1, 0.2, 0.3, 0.4, 0.5, 0.6, 0.7, 0.8, 0.9, 1.0 V s^{-1}). (B) The relationships of E_{pa} (a) and E_{pc} (b) with log v.

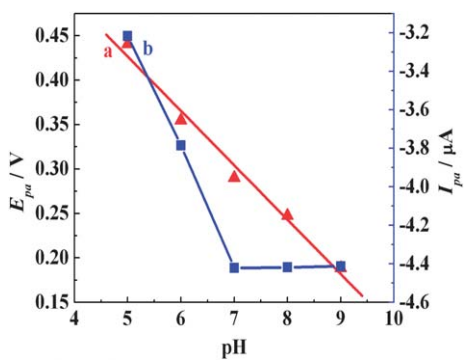

Fig. 7 The relationship of E_{pa} (a) and I_{pa} (b) against pH (scan rate: 0.1 V s^{-1}).

3.6 pH effect

The effect of buffer pH on the current response of 0.5 mM phosphate buffer solution on the CDs–CS/GCE was investigated in a pH range from 5.0 to 9.0 by CV, the results are shown in Fig. 7. The oxidation peak potential shifted negatively with the increase of pH value, indicating that protons were involved in the electrode reaction. A good linear relationship between E_{pa} and pH was constructed with a linear regression equation of E_{pa} (V) = −0.0612 pH + 0.732 (R = −0.992). The slope value of −61.2 mV pH^{-1} shows that the electron transfer was accompanied by an equal number of protons.[23]

At the same time, when the pH value increased from 5.0 to 7.0, the anodic peak current of DA increased. Nevertheless, when the pH was beyond 7.0, the peak current conversely decreased. This phenomenon was probably due to the dissociation of the phenolic moiety to produce the corresponding anion. Therefore, considering the sensitive determination for DA, a phosphate buffer solution of pH = 7.0 was chosen for the subsequent analytical experiments.

3.7 Interference effect

As we know, using a bare GCE, the oxidation peak potentials for ascorbic acid (AA), uric acid (UA) and DA are very close to each other and thus it is difficult to separate these compounds due to their overlapping signals.[35] This problem can be eliminated by electrostatic attraction, since the CDs–CS film, which is in its anionic form at the working electrode's surface in the pH 7.0 phosphate buffer solution, both AA (pK_a = 4.1) and UA (pK_a = 5.75) are negatively charged, but DA (pK_a = 8.89) is positively charged at physiological pH (7.0) (ref. 36 and 37). So, CDs–CS, as a cationic exchanger at the GCE's surface selectively attracts cationic DA and allows them to pass through to the electrode's surface. Meanwhile, CDs–CS prevents anionic AA and UA from reaching the electrode's surface. As a result, AA and UA did not exchange electrons with the electrode. As shown in Fig. 8, it could be concluded that the presence of AA (A) and UA (B) did not interfere in DA determination.

In addition, other influences from common co-existing substances were also investigated. When the relative error (Er) exceeded 5%, each matter was considered as an interfering agent. It was found that most ions and common substances at high concentration only caused a negligible change: Na^+, K^+, Cl^-, NO_3^-, SO_4^{2-} (>500 fold), Ca^{2+}, Zn^{2+}, Mg^{2+}, Pb^{2+} (200 fold), lysine, cysteine, glucose (150 fold), serotonin (100 fold) and norepinephrine (10 fold). The results indicate the CDs–CS/GCE exhibits good selectivity for DA detection.

3.8 Calibration plot and limit of detection

By using the more sensitive differential pulse voltammetry (DPV) as the detection method, the CDs–CS/GCE was further used for the DA detection. Under optimal conditions, the oxidation peak current of DA increased with its concentration in the range from 0.1 μM to 30 μM with typical DPV shown in Fig. 9, which had a linear regression equation of I_{pa} (μA) = −0.0212C (μM) − 0.04611 (R = 0.996). The detection limit was calculated as 11.2 nM, which was lower than some previous reports (Table 1), which illustrates that the CDs–CS/GCE has good sensitivity and a wide linear range. The electrode was put into a vacuum drying oven at 25 °C, and DA samples were determined every 48 hours. Fig. 10 shows that the electrode has a wonderful stability after two weeks.

3.9 Application of the probe

In order to evaluate the applicability of the proposed method to the determination of DA in pharmaceutical preparations, we examined this ability by differential pulse voltammetric determination of DA concentration in an injection solution based on the repeated differential pulse voltammetric responses (n = 5) of the diluted analytes and the samples that were spiked with a specified concentration of DA. Using the standard addition method, measurements were made of DA concentrations in the pharmaceutical preparations and of the recovery rate of the spiked samples. The results are listed in Table 2.

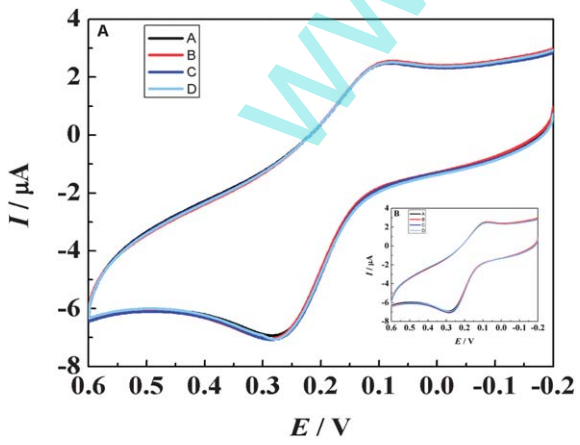

Fig. 8 CV of 0.2 mM DA with the different concentrations of AA, A: 0 mM (A), 2.0 mM (B), 20.0 mM (C), 30.0 mM (D); and UA, B: 0 mM (A), 2.0 mM (B), 20.0 mM (C), 30.0 mM (D).

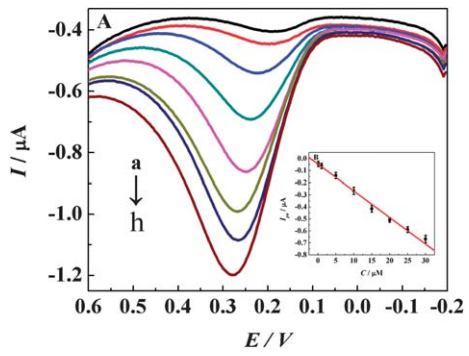

Fig. 9 (A) DPV of DA with increasing concentration (from a to h: 0.1, 1.0, 5.0, 10.0, 15.0, 20.0, 25.0, 30.0 μM). (B) The relationship of I_{pa} with the concentration of DA.

Table 1 Comparison of the analytical performances of different modified electrodes

Electrode	Linear range (μM)	Detection limit (μM)	References
GME	4.0–100	2.64	14
MPEG	2.0–140	0.0468	15
HNCMS/GC	3.0–7.5	0.02	16
Cu_2O/graphene	0.1–10	0.01	17
AuNP/PANI	3.0–20	—	18
TBQ/MCPE	10–100	—	19
NPG/ITO	1.5–27.5	1.5	20
f-MWCNTs	3.0–300	—	21
PPy/eRGO	0.1–150	0.023	22
TA-SAM	1.5–100	0.5	23
OCMCS	0.06–7.0	0.0015	24
CDs–CS/GCE	0.1–30	0.0112	This work

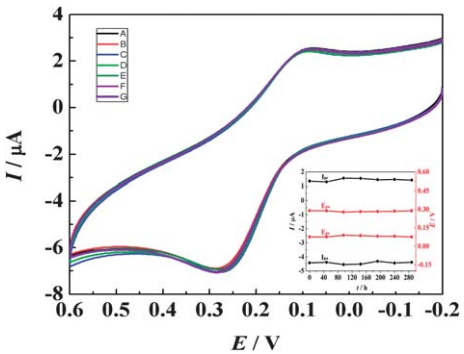

Fig. 10 CV of 0.2 mM DA recorded on the CDs–CS/GCE with increasing time (from A to G: 0, 48, 96, 144, 192, 240, 288 h).

Table 2 Results of determination of DA in its injection solution

Sample (μM)	Found (μM)	Spiked (μM)	Total found (μM)	Recovery (%)
10	9.96	5.0	15.01	101.0
10	10.01	5.0	14.98	99.4
10	9.95	5.0	14.97	100.4
10	10.03	5.0	15.01	99.6
10	9.97	5.0	14.92	99.0

4 Conclusions

In this study, an electrochemical method was developed and successfully applied for the determination of DA. Under optimal conditions, the CDs–CS/GCE showed better electrochemical response towards the detection of DA than the GCE, a linear relationship between the oxidation peak current of DA and its concentration can be obtained in a range from 0.1 μM to 30.0 μM with the limit of detection as 11.2 nM (3*S*/*N*). The CDs–CS/GCE was applied to the detection of DA content in injection solutions of DA with satisfactory results.

Acknowledgements

This project was supported by the science and technology foundation of the national general administration of quality supervision in China (2012QK053) and Fujian province natural science foundation (2012D136).

References

1 X. Ji, G. Palui, T. Avellini, H. B. Na, C. Yi, K. L. Knappenberger and H. Mattoussi, *J. Am. Chem. Soc.*, 2012, **134**, 6006–6017.
2 L. D. Morgan, H. Baker, M. S. Yeoman and B. A. Patel, *Analyst*, 2012, **137**, 1409–1415.
3 A. Dalpiaz, B. Cacciari, C. B. Vicentini, F. Bortolotti, G. Spalluto, S. Federico, B. Pavan, F. Vincenzi, P. A. Borea and K. Varani, *Mol. Pharmaceutics*, 2012, **9**, 591–604.
4 D. Sulzer, *Neuron*, 2011, **69**, 628–649.
5 P. E. Phillips, G. D. Stuber, M. L. Heien, R. M. Wightman and R. M. Carelli, *Nature*, 2003, **422**, 614–618.
6 C. Muzzi, E. Bertocci, L. Terzuoli, B. Porcelli, I. Ciari, R. Pagani and R. Guerranti, *Biomed. Pharmacother.*, 2008, **62**, 253–258.
7 V. Carrera, E. Sabater, E. Vilanova and M. A. Sogorb, *J. Chromatogr., B: Anal. Technol. Biomed. Life Sci.*, 2007, **847**, 88–94.
8 W. J. Barreto, S. R. Barreto, R. A. Ando, P. S. Santos, E. DiMauro and T. Jorge, *Spectrochim. Acta, Part A*, 2008, **71**, 1419–1424.
9 H. Li, C. Li, Z. Y. Yan, J. Yang and H. Chen, *J. Neurosci. Methods*, 2010, **189**, 162–168.
10 J. R. Thabano, M. C. Breadmore, J. P. Hutchinson, C. Johns and P. R. Haddad, *J. Chromatogr., A*, 2009, **1216**, 4933–4940.
11 J. B. Chien, R. A. Wallingford and A. G. Ewing, *J. Neurochem.*, 1990, **54**, 633–638.
12 H. Y. Wang, Y. Sun and B. Tang, *Talanta*, 2002, **57**, 899–907.
13 J. L. Chen, X. P. Yan, K. Meng and S. F. Wang, *Anal. Chem.*, 2011, **83**, 8787–8793.
14 Y. R. Kim, S. Bong, Y. J. Kang, Y. Yang, R. K. Mahajan, J. S. Kim and H. Kim, *Biosens. Bioelectron.*, 2010, **25**, 2366–2369.
15 M. Liu, L. Wang, J. Deng, Q. Chen, Y. Li, Y. Zhang, H. Li and S. Yao, *Analyst*, 2012, **137**, 4577–4583.
16 C. Xiao, X. Chu, Y. Yang, X. Li, X. Zhang and J. Chen, *Biosens. Bioelectron.*, 2011, **26**, 2934–2939.
17 F. Zhang, Y. Li, Y. Gu, Z. Wang and C. Wang, *Microchim. Acta*, 2011, **173**, 103–109.
18 A. Stoyanova, S. Ivanov, V. Tsakova and A. Bund, *Electrochim. Acta*, 2011, **56**, 3693–3699.
19 H. R. Zare, N. Nasirizadeh and M. Mazloum Ardakani, *J. Electroanal. Chem.*, 2005, **577**, 25–33.
20 P. Y. Ge, Y. Du, J. J. Xu and H. Y. Chen, *J. Electroanal. Chem.*, 2009, **633**, 182–186.
21 Z. A. Alothman, N. Bukhari, S. M. Wabaidur and S. Haider, *Sens. Actuators, B*, 2010, **146**, 314–320.
22 P. Si, H. Chen, P. Kannan and D. H. Kim, *Analyst*, 2011, **136**, 5134–5138.
23 Y. Sun and F. W. Sheng, *Microchim. Acta*, 2006, **154**, 115–121.
24 C. Y. Wang, Z. X. Wang, A. P. Zhu and X. Y. Hu, *Sensors*, 2006, **6**, 1523–1536.
25 M. L. A. V. Heien, P. E. M. Phillips, G. D. Stuber, A. T. Seipel and R. M. Wightman, *Analyst*, 2003, **128**, 1413–1419.

26 E. L. Ciolkowski, K. M. Maness, P. S. Cahlil, R. M. Wightman, D. H. Evans, B. Fosset and C. Amatore, *Anal. Chem.*, 1994, **66**, 3611–3617.
27 H. Zhu, X. Wang, Y. Li, Z. Wang, F. Yang and X. Yang, *Chem. Commun.*, 2009, 5118–5120.
28 J. M. Liu, L. P. Lin, X. X. Wang, S. Q. Lin, W. L. Cai, L. H. Zhang and Z. Y. Zheng, *Analyst*, 2012, **137**, 2637–2642.
29 H. Dai, G. Xu, L. Gong, C. Yang, Y. Lin, Y. Tong, J. Chen and G. Chen, *Electrochim. Acta*, 2012, **80**, 362–367.
30 B. Chen, F. Li, S. Li, W. Weng, H. Guo, T. Guo, X. Zhang, Y. Chen, T. Huang, X. Hong, S. You, Y. Lin, K. Zeng and S. Chen, *Nanoscale*, 2013, **5**, 1967–1971.
31 B. Rezaei and S. Damiri, *Sens. Actuators, B*, 2008, **134**, 324–331.
32 B. Ge, Y. Tan, Q. Xie, M. Ma and S. Yao, *Sens. Actuators, B*, 2009, **137**, 547–554.
33 F. C. Anson, *Anal. Chem.*, 1964, **36**, 932–934.
34 E. Laviron, *J. Electroanal. Chem.*, 1979, **101**, 19–28.
35 L. Liu, S. Li, L. Liu, D. Deng and N. Xia, *Analyst*, 2012, **137**, 3794–3799.
36 M. Zhang, K. Gong, H. Zhang and L. Mao, *Biosens. Bioelectron.*, 2005, **20**, 1270–1276.
37 S. C. Fernandes, I. C. Vieira, R. A. Peralta and A. Neves, *Electrochim. Acta*, 2010, **55**, 7152–7157.